Two-pore channels (TPCs) acts as a hub for excitation-contraction coupling, metabolism and cardiac hypertrophy signalling

Antoine de Zélicourt, Abdallah Fayssoil, Arnaud Mansart, Faouzi Zarrouki, Ahmed Karoui, Jérome Piquereau, Florence Lefebvre, Pascale Gerbaud, Delphine Mika, Mbarka Dakouane-Giudicelli, et al.

Cell Calcium 117 (2024) 102839

Contents lists available at ScienceDirect

Cell Calcium

journal homepage: www.elsevier.com/locate/ceca

Two-pore channels (TPCs) acts as a hub for excitation-contraction coupling, metabolism and cardiac hypertrophy signalling

Antoine de Zélicourt [a,b], Abdallah Fayssoil [a], Arnaud Mansart [c], Faouzi Zarrouki [b], Ahmed Karoui [d], Jérome Piquereau [d], Florence Lefebvre [d], Pascale Gerbaud [d], Delphine Mika [d], Mbarka Dakouane-Giudicelli [a], Erwan Lanchec [b,h], Miao Feng [g], Véronique Leblais [d], Régis Bobe [g], Jean-Marie Launay [e], Antony Galione [f], Ana Maria Gomez [d,1], Sabine de la Porte [a,1], José-Manuel Cancela [b,1,*]

[a] Université Paris-Saclay, UVSQ, Inserm, END-ICAP, 78000 Versailles, France
[b] Neuroscience Paris-Saclay Institute (Neuro-PSI), UMR 9197, CNRS- Université Paris-Saclay, Saclay, 91400, France
[c] Université Paris-Saclay, UVSQ, Inserm, 2I, 78000 Versailles, France
[d] UMR-S 1180, INSERM, Signaling and cardiovascular pathophysiology, Université Paris-Saclay, 91400 Orsay, France
[e] Service de Biochimie, INSERM UMR S942, Hôpital Lariboisière, Paris, France
[f] Department of Pharmacology, University of Oxford, Oxford OX1 3QT, United Kingdom
[g] UMR-S 1176, Université Paris-Saclay, Le Kremlin Bicêtre, France

ARTICLE INFO

Keywords:
Ca^{2+}
TPC
NAADP
Cardiomyopathies
Cardiomyocytes
Endo-lysosome

ABSTRACT

Ca^{2+} signaling is essential for cardiac contractility and excitability in heart function and remodeling. Intriguingly, little is known about the role of a new family of ion channels, the endo-lysosomal non-selective cation "two-pore channel" (TPCs) in heart function. Here we have used double TPC knock-out mice for the 1 and 2 isoforms of TPCs (*Tpcn1/2*$^{-/-}$) and evaluated their cardiac function. Doppler-echocardiography unveils altered left ventricular (LV) systolic function associated with a LV relaxation impairment. In cardiomyocytes isolated from *Tpcn1/2*$^{-/-}$ mice, we observed a reduction in the contractile function with a decrease in the sarcoplasmic reticulum Ca^{2+} content and a reduced expression of various key proteins regulating Ca^{2+} stores, such as calsequestrin. We also found that two main regulators of the energy metabolism, AMP-activated protein kinase and mTOR, were down regulated. We found an increase in the expression of TPC1 and TPC2 in a model of transverse aortic constriction (TAC) mice and in chronically isoproterenol infused WT mice. In this last model, adaptive cardiac hypertrophy was reduced by Tpcn1/2 deletion. Here, we propose a central role for TPCs and lysosomes that could act as a hub integrating information from the excitation-contraction coupling mechanisms, cellular energy metabolism and hypertrophy signaling.

1. Introduction

Amongst the many signaling pathways involved in cardiac regulation, Ca^{2+} signaling plays a central role in the excitation-contraction coupling (ECC), through Ca^{2+}-induced Ca^{2+} release (CICR) [1]. Most studies have focused on the SR as a Ca^{2+} store involved in CICR and surprisingly, lysosomes, which forms close contacts with mitochondria and SR, have been poorly investigated as a Ca^{2+} store. An important Ca^{2+}-releasing messenger [2,3] and regulator of the ECC in cardiomyocytes following ß-Adrenergic receptor stimulation [4–7] is nicotinic acid dinucleotide phosphate (NAADP). Recently, several studies have demonstrated that the endo-lysosomal non-selective cation channel "two-pore channel" (TPC) is required for NAADP-induced Ca^{2+} release from endo-lysosomal Ca^{2+} stores in various cell types [8–12]. TPCs belong to the superfamily of voltage-gated ion channels and were originally identified in animals and plants on the basis of sequence identity with voltage-gated Ca^{2+} and Na^{+} channels [13]. In rodents and humans, there are two isoforms of TPCs, TPC1 and TPC2. In animals,

* Corresponding author.
E-mail address: jose-manuel.cancela@universite-paris-saclay.fr (J.-M. Cancela).
[h] Sherbrooke University, Dept. of Physiology & Pharmacology, QC, Canada
[1] Co-senior authors contributed equally to the work.

https://doi.org/10.1016/j.ceca.2023.102839
Received 12 September 2023; Received in revised form 1 December 2023; Accepted 2 December 2023
Available online 16 December 2023

TPC2 is predominantly expressed on lysosomes and late endosomes, whereas TPC1 is expressed throughout the endo-lysosomal system. Studies have suggested that TPC1 and TPC2 could be modulated by other factors than NAADP, such as the lipid phosphatidylinositol 3, 5-bisphosphate ($PI(3,5)P_2$), mammalian target of rapamycin (mTOR), ATP, or nutrient levels [14–17]. It has also been reported that TPCs carry Na^+ currents when activated by $PI(3,5)P_2$ in endo-lysosomes excised from cell lines overexpressing TPC1 or TPC2, whereas increased Ca^{2+}permeability is associated with their regulation by NAADP. Regulation of gating and ionic selectivity of TPC1 and TPC2 have been shown to be different, with TPC1 being more permeable to protons than K^+, Na^+, or Ca^{2+}, whereas TPC2 is more permeable to Ca^{2+} and Na^+ [14, 18–20].

There are also several lines of evidence that TPCs are functionally highly relevant to the modulation of cardiac function. Deletion of TPC2, but not TPC1, reduces ß-adrenergic modulation of Ca^{2+} transients in isolated cardiomyocytes and protects the heart from isoproterenol-induced hypertrophy and arrhythmia [5,21]. Additionally, a recent study clearly shows that inhibition of NAADP signaling on reperfusion following ischemia protects the heart by preventing lethal calcium oscillations via its action on TPC1 [22]. All these studies suggest that TPCs deletion or inhibition could be beneficial, but intriguingly, in human left ventricular failing myocardium, the expression of the two isoforms TPC1 and TPC2 is increased [17]. This last result suggests that modulation of TPCs expression might be central to the cardiac function. Thus, the consequences of down or up-regulation of the TPC1 and TPC2 expression in cardiac function and dysfunction is poorly known. Here, we have explored for the first time the consequence of the full deletion of the two isoforms of TPCs on the basal cardiac function and whether TPCs expression could be up regulated in two mouse models of adaptive cardiac hypertrophy.

We have used constitutive full body TPC double knock-out mice (*Tpcn1/2*$^{-/-}$). These are viable and grow normally. By performing the evaluation of the cardiac function, we unveiled moderate systolic and diastolic alterations, with normal ECG profiles, showing that TPCs are important for the cardiac contraction. At the cardiomyocyte level, we observed a decrease in the contractile function as well as in the sarcoplasmic reticulum Ca^{2+} content. These defects were associated with reduced expression of the ryanodine receptors (RyR2), calsequestrin (CSQ) and an increased expression of the cardiac troponin I (cTnI).

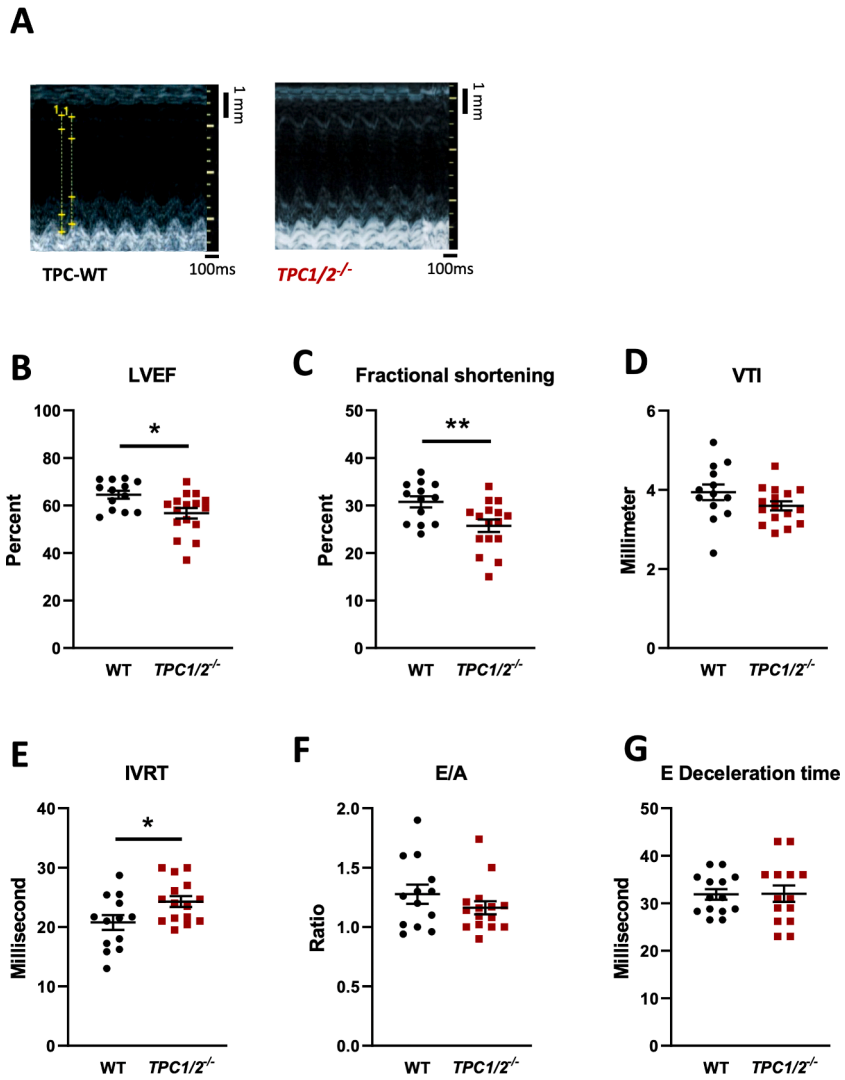

Fig. 1. Alteration of the cardiac function in *Tpcn1/2*$^{-/-}$ mice. (A) Typical time motion (TM) mode echocardiography of the left ventricle of WT versus *Tpcn1/2*$^{-/-}$ mice, from a parasternal short axis view. **(B)** Left ventricular ejection fraction (LVEF, $N = 13$ WT mice, $N = 16$ *Tpcn1/2*$^{-/-}$ mice). Significance was assessed using a *t*-test. **(C)** Fractional shortening ($N = 13$ WT mice, $N = 16$ *Tpcn1/2*$^{-/-}$ mice). Significance was assessed using a *t*-test **(D)** Subaortic velocity time integral (VTI, $N = 13$ WT mice, $N = 16$ *Tpcn1/2*$^{-/-}$ mice) **(E)** Isovolumic relaxation time (IVRT, $N = 13$ WT mice, $N = 16$ *Tpcn1/2*$^{-/-}$ mice). Significance was assessed using a *t*-test. **(F)** E/A ratio ($N = 13$ WT mice, $N = 16$ *Tpcn1/2*$^{-/-}$ mice**) (G)** Deceleration time of the E wave ($N = 13$ WT mice, $N = 14$ *Tpcn1/2*$^{-/-}$ mice). Fig. 1, each dot of the graphs represents the parameters recorded in a single mouse. Each dot is the mean of duplicates. Values are expressed as mean ± SEM. *$p<0.05$, **$p<0.01$, ***$p<0.001$.

Additionally, we found that regulators of the energy metabolism are down regulated in *Tpcn1/2*$^{-/-}$ mice suggesting a poor ability to adapt to energy requirement such as during sustained effort or cell growth. Indeed, we also showed that despite a normal limb strength and respiratory function, *Tpcn1/2*$^{-/-}$ mice displayed a poor performance in a treadmill exhaustion test. Finally, we found an increased expression of TPC1 and TPC2 in two models of cardiac hypertrophy, namely the TAC (transverse aorta constriction) model and chronically isoproterenol-injected WT mice. In this last model, adaptive cardiac hypertrophy was reduced in *Tpcn1/2*$^{-/-}$ mice chronically injected with isoproterenol.

2. Results

2.1. *Tpcn1/2*$^{-/-}$ mice display systolic and diastolic function alterations

We addressed the role of TPCs in heart function by performing Doppler-echocardiography in 2-month-old *Tpcn1/2*$^{-/-}$ mice (Fig. 1) which revealed significant left ventricular (LV) dysfunction. Concerning the systolic function, hearts from *Tpcn1/2*$^{-/-}$ mice displayed a decrease in the LV ejection fraction (LVEF) and a reduced LV fractional shortening (FS) (Fig. 1A-C), without any change in subaortic velocity time integral (VTI) (Fig. 1D). Concerning the LV diastolic function, *Tpcn1/2*$^{-/}$

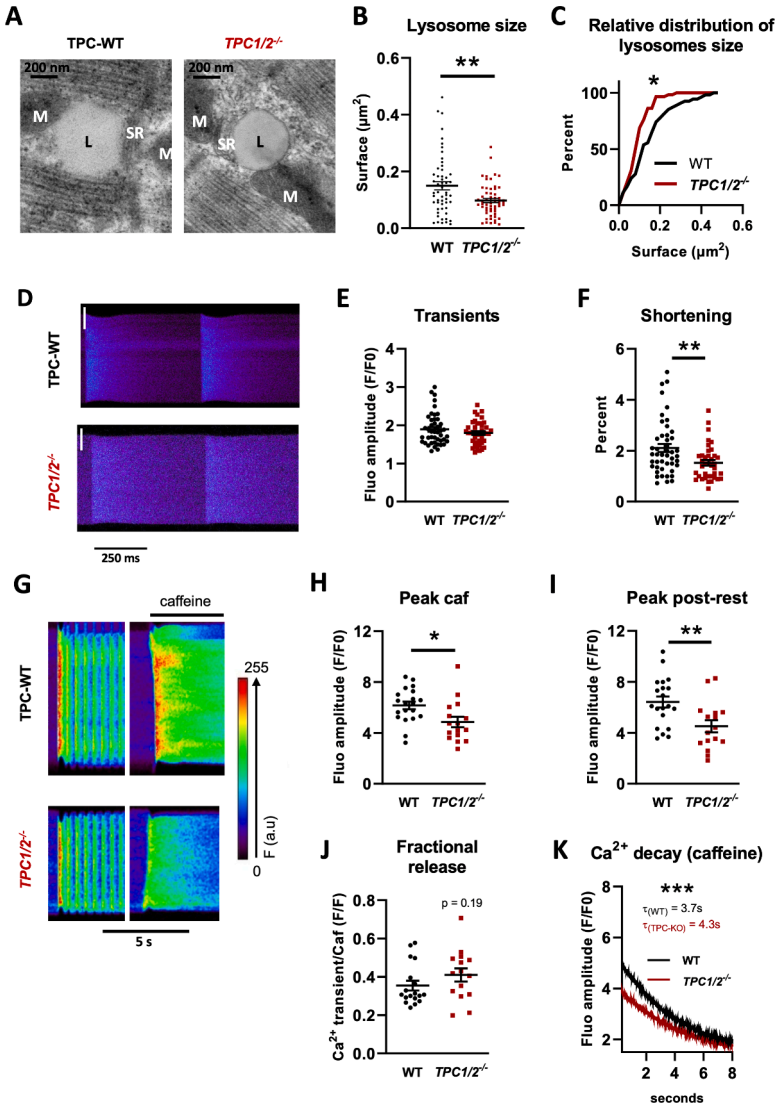

Fig. 2. Isolated cardiomyocytes from *Tpcn1/2*$^{-/-}$ mice display reduced cell shortening and Ca^{2+} content in the SR. (A) Magnify electron micrograph of cardiomyocytes from WT mice and *Tpcn1/2*$^{-/-}$ mice showing lysosomes (L), Sarcoplasmic reticulum (SR) and mitochondria (M). **(B)** Size of lysosomes was determined by the measure of their surface in µm^2. Each dot of the graph represents a lysosome ($n = 54$ lysosomes obtained from WT mice ($N = 3$ mice) and $n = 58$ lysosomes obtained from *Tpcn1/2*$^{-/-}$ mice ($N = 3$ mice)). Significance was assessed using a Mann-Whitney test **(C)** Relative cumulative distribution (in percent) of lysosome size **(D)** Line scanning confocal images showing Ca^{2+} transient evoked by 2 Hz electrical stimulations in cardiomyocytes. Scale bar, 20 µm **(E)** Transient fluorescence amplitude ($n = 44$ cells/ $N = 4$ WT mice; $n = 42$ cells/$N = 4$ *Tpcn1/2*$^{-/-}$ mice) **(F)** Cell shortening following electrical stimulation ($n = 46$ cells/ $N = 4$ WT mice; $n = 38$ cells/$N = 4$ *Tpcn1/2*$^{-/-}$ mice). Significance was assessed using a Mann-Whitney test.**(G)** Line scanning confocal images showing electrical stimulations and caffeine Ca^{2+} responses in cardiomyocytes. **(H)** Fluorescence amplitude of the Ca^{2+} transient evoked by 10 mM caffeine ($n = 20$ cells/ $N = 4$ WT mice; $n = 16$ cells/$N = 4$ *Tpcn1/2*$^{-/-}$ mice). Significance was assessed using a *t*-test. **(I)** Amplitude of the peak post-rest ($n = 20$ cells/ $N = 4$ WT mice; $n = 16$ cells/$N = 4$ *Tpcn1/2*$^{-/-}$ mice). Significance was assessed using a *t*-test. **(J)** Fractional release value ($n = 18$ cells/ $N = 4$ WT mice; $n = 15$ cells/$N = 4$ *Tpcn1/2*$^{-/-}$ mice). **(K)** Curves showing the mean Ca^{2+} decay after the caffeine-evoked Ca^{2+}peak, in WT and *Tpcn1/2*$^{-/-}$ isolated cardiomyocytes ($n = 20$ cells/ $N = 4$ WT mice; $n = 16$ cells/$N = 4$ *Tpcn1/2*$^{-/-}$ mice). The fitting curve equations have been determined by non-linear regression and significance of the decay constants K was assessed using the least squares fit method. For the Fig. 2, each dot of the graphs represents the value of a single cardiomyocyte recorded from $N = 4$ WT mice and $N = 4$ *Tpcn1/2*$^{-/-}$ mice. Values are expressed as mean ± SEM and significance: *$p<0.05$, **$p<0.01$, ***$p<0.001$.

$^{-}$ hearts also displayed LV relaxation impairment with an increase in the intra-volumic relaxation time (IVRT), an index of diastolic function (Fig. 1E). We did not see abnormality of the E/A ratio (velocities of early filling peak (E wave) and late diastolic filling (A wave) peak) and the mitral deceleration time was not different from the value recorded in WT mice (Fig. 1F and G). This impairment of LV diastolic function in *Tpcn1/2*$^{-/-}$ mice was not related to heart rate (HR) (Figure S1B) nor to electrocardiogram parameters (ECG) (Figure S1A-E) since no significant differences were observed.

2.2. *Tpcn1/2*$^{-/-}$ cardiomyocytes have no structural alterations but display reduced lysosomes size

Despite the cardiac abnormalities, the *Tpcn1/2*$^{-/-}$ mice were viable and Masson's trichrome staining did not reveal any major differences in heart fibrosis from *Tpcn1/2*$^{-/-}$ mice compared with WT mice up to 26 months old (Figure S2A$_1$,A$_2$). This finding was corroborated by the absence of heart hypertrophy evaluated post-sacrifice by the heart weight to body weight ratio (Figure S2B). The echocardiography revealed no structural changes and an absence of left ventricular (LV) dilation or hypertrophy (Figure S2C). Finally, since TPCs have been involved in muscular differentiation, we performed electron microscopy experiments to assess whether TPCs deletion impaired cardiomyocytes ultrastructure. Electron micrographs did not show any significant differences in cardiomyocytes from *Tpcn1/2*$^{-/-}$ mice compared with those from WT mice (Figure S2D). However, knowing that endo-lysosomes and TPCs may functionally and structurally interact at membrane contact sites with the SR, a key component of the ECC process, we made a structural analysis by performing and electron microscopic experiment and showed that lysosomes, SR and mitochondria form microdomains as previously reported [23], with no apparent structural abnormality in *Tpcn1/2*$^{-/-}$ mice (Fig. 2A). Nevertheless, lysosomes size is significantly reduced by around 35 % in *Tpcn1/2*$^{-/-}$ mice (Fig. 2B,C) whereas the proportion of lysosomes forming membrane contact sites or close appositions (<50 nm) with the SR was found to be identical between WT and *Tpcn1/2*$^{-/-}$ mice (Figure S4A).

2.3. *Tpcn1/2*$^{-/-}$ cardiomyocytes display reduced cell shortening

To determine whether Ca^{2+} signaling is altered in *Tpcn1/2*$^{-/-}$ mice, confocal Ca^{2+} imaging experiments were performed in electrically stimulated cardiomyocytes isolated from 2-month-old *Tpcn1/2*$^{-/-}$ mice (Fig. 2D). We observed no change in the amplitude of the electrically-evoked Ca^{2+} transient, but a significant reduction in cell shortening in *Tpcn1/2*$^{-/-}$ myocytes compared with the WT values (Fig. 2E and F). Ca^{2+} sparks and Ca^{2+} waves frequencies were measured as an index of RyR activity. No differences were observed in the percentage of active cells (Figure S3C) or in the frequencies of either Ca^{2+} sparks, waves or triggered activity (spontaneous full Ca^{2+} transients) (Figure S3D), suggesting that RyRs function was not apparently altered in *Tpcn1/2*$^{-/-}$ mice.

2.4. *Tpcn1/2*$^{-/-}$ cardiomyocytes display reduced SR Ca^{2+} content

Knowing that the electrically evoked cell shortening is reduced and the RyR2 activity is dependent on the amount of Ca^{2+} stored, we looked at whether a decrease in the SR Ca^{2+} content is maintained. The Ca^{2+} load of the SR was assessed by rapid caffeine application (Fig. 2G). Cardiomyocytes from *Tpcn1/2*$^{-/-}$ mice showed a reduced amplitude of the caffeine-induced Ca^{2+} peak compared with WT cardiomyocytes, suggesting a reduced SR Ca^{2+} content in *Tpcn1/2*$^{-/-}$ mice (Fig. 2H). The amplitude of the peak after rest (peak post-rest) was also reduced in *Tpcn1/2*$^{-/-}$ mice, which also suggests a reduction in the filling state of SR Ca^{2+} stores (Fig. 2I). The fractional release value tended to be increased, suggesting that the RyRs sensitivity might be moderately higher in *Tpcn1/2*$^{-/-}$ cardiomyocytes (Fig. 2J). Finally, the Ca^{2+} transient decay time of the caffeine response was slower in *Tpcn1/2*$^{-/-}$ than in WT mice, suggesting that Na^{+}/Ca^{2+} exchanger (NCX) activity could be impaired by TPCs deletion (Fig. 2K).

2.5. *Tpcn1/2*$^{-/-}$ heart have reduced SR protein expression

Thus, to further explore the consequences of TPCs deletion on Ca^{2+} signaling impairments described above, we assessed by western blot in *Tpcn1/2*$^{-/-}$ mice the expression of key proteins involved in the ECC. We found a slight reduction in RyR2 expression (Fig. 3A) with no difference in the phosphorylated RyR ratio (Figure S4B,C) and Cav 1.2 (Fig. 3B) expression. Furthermore, TPCs deletion resulted in a significant reduction in NCX expression (Fig. 3C), which agrees with the slower decay time observed in the caffeine response (Fig. 2J). Importantly, our results clearly showed a reduction in the expression of CSQ2 (Fig. 3D), the main SR Ca^{2+} binding protein, whereas the SERCA2 pump (Fig. 3E), the phospholamban (PLB) expression (Figure S4D) and the ratio P-PLB/PLB total (Figures S4E,F) were unchanged. Finally, the impairment of LV relaxation in *Tpcn1/2*$^{-/-}$ mice and decreased unloaded cell contraction prompted us to look at c-TnI, a protein of the troponin complex, another important component of ECC regulation. In agreement with the alteration of the LV relaxation, we found that the cardiac c-TnI level was increased in *Tpcn1/2*$^{-/-}$ mice (Fig. 3F) whereas the troponin C levels were unchanged (Figure S4G).

2.6. *Tpcn1/2*$^{-/-}$ heart have reduced expression in metabolic regulators

As described in the present work (Figs. 2A and 4A) and in previous studies [23,24], cardiomyocyte structural organization shows a proximity between organelles such as mitochondria and lysosomes, thereby allowing the establishment of Ca^{2+} and energy microdomains between these organelles. Our electron microscopy experiments also showed that lysosomes form membrane contact sites or close appositions (<50 nm) with mitochondria in the two mouse strains. Surprisingly, TPCs deletion led to an increase in the proportion of lysosomes involved in such contact sites (Fig. 4A). Since mitochondria are central to energy metabolism, we evaluated their function. In the *Tpcn1/2*$^{-/-}$ mice, the mitochondrial mass was similar to WT mice, as judged by citrate synthase activity (Figure S5A) whereas we found a moderate increase in the activity of complex I of the respiratory chain without any change in complex IV activity or in mitochondrial electron transfer chain capacities suggesting that mitochondria function is normal in *Tpcn1/2*$^{-/-}$ mice (Figure S5B). It is documented that deletion of TPCs in cardiomyocytes impaired starvation-induced autophagy a process regulated by both AMPK, a sensor of the ATP status and mTOR, an autophagy and protein synthesis regulator [25]. Two modulators required to adapt to the energy demand.

To confirm that TPCs deletion could altered on energy metabolism adaptation, we determined by RT-qPCR the expression of 3 key regulators: AMPK, mTOR and PGC1-α, a transcriptional factor regulating mitogenesis [26]. Interestingly, we found that in *Tpcn1/2*$^{-/-}$ mice, AMPK (Fig. 4B) and mTOR (Fig. 4C) were both downregulated, whereas PGC1-α expression (Fig. 4D) remained unchanged. To evaluate whether *Tpcn1/2*$^{-/-}$ mice have the ability to sustain an energy de-manding effort, we first analyzed whether the *Tpcn1/2*$^{-/-}$ mice phenotype for skeletal muscle function could be impaired. We found that *Tpcn1/2*$^{-/-}$ mice displayed a normal limb strength (Fig. 4E) and the skeletal muscle of the limb from *Tpcn1/2*$^{-/-}$ mice displayed neither fibrosis or histological defects (Fig. 4F, S5E). We also found using plethysmography that *Tpcn1/2*$^{-/-}$ mice displayed normal respiratory function (Fig. 4G,H,I). We then challenged the *Tpcn1/2*$^{-/-}$ mice for evaluating the endurance of these mice with a more energy demanding exercise namely the treadmill exhaustion test and indeed, we found that in absence of TPCs, the mice were unable to sustain a long effort, with very significant reductions in the running time (Fig. 4J), the maximum speed reached (Figure S5C) and the distance run (Figure S5D) compared with the WT

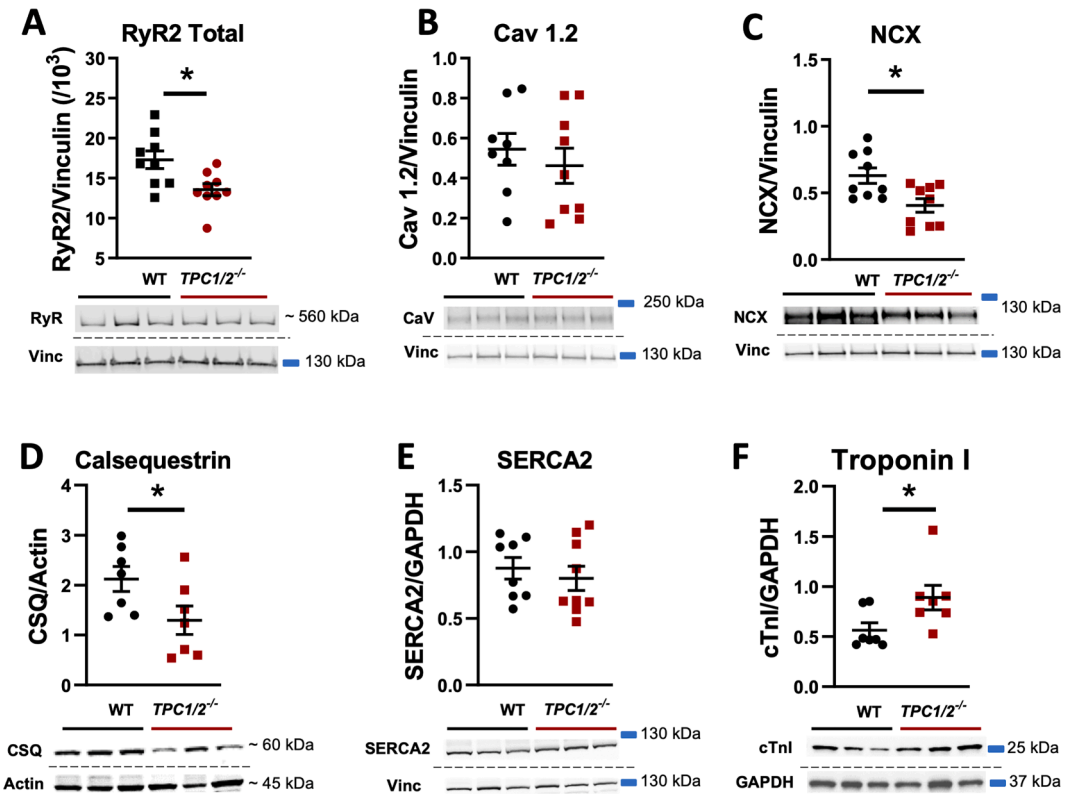

Fig. 3. ***Tpcn1/2*$^{-/-}$ cardiomyocytes display smaller lysosomes and reduced SR protein expression.** **(A)** Western blot of total heart ryanodine receptors (RyR2, $N = 9$ WT mice; $N = 9$ *Tpcn1/2*$^{-/-}$ mice). Significance was assessed using a *t*- test. **(B)** Western blot of heart l-type calcium channel (CaV 1.2, $N = 8$ WT mice; $N = 9$ *Tpcn1/2*$^{-/-}$ mice). **(C)** Western blot of heart Na^+/Ca^{2+} exchanger (NCX, $N = 7$ WT mice; $N = 7$ *Tpcn1/2*$^{-/-}$ mice). Significance was assessed using a Mann-Whitney test. **(D)** Western blot of heart calsequestrin (CSQ, $N = 7$ WT mice; $N = 7$ *Tpcn1/2*$^{-/-}$ mice), significance was assessed using a *t*-test **(E)** Western blot of heart SERCA2 pumps ($N = 8$ WT mice; $N = 9$ *Tpcn1/2*$^{-/-}$ mice). Significance was assessed using a Mann-Whitney test. **(F)** Western blot of heart troponin I (c-TnI, $N = 7$ WT mice; $N = 7$ *Tpcn1/2*$^{-/-}$ mice). Significance was assessed using a Mann-Whitney test. Each dot of the graphs represents a single mouse. Values are expressed as mean ± SEM and significance: $*p<0.05$, $**p<0.01$, $***p<0.001$.

mice. The reduced endurance of the *Tpcn1/2*$^{-/-}$ mice is consistent with the reduction in the AMPK expression and previous report, as AMPK plays key roles in the maintenance of the energy homeostasis, especially when the energy demand increases [27].

2.7. Heart hypertrophy in a chronically isoproterenol injected mouse model increased the expression of TPCs and their deletion reduced hypertrophy

Adaptive cardiac hypertrophy is an important aspect where the energy status and AMPK/mTOR pathways are required for regulating cell growth. We therefore investigated the role and expressions of TPCs in two mouse models of heart hypertrophy, namely a chronic exposure to isoproterenol in WT mice and the transverse aortic constriction (TAC) model (see [28] for details). RT-qPCR expression of TPC1 and TPC2 was found to be increased by 2 to 3-fold, in both TAC mice (Fig. 5A and B) and in chronically isoproterenol-injected WT mice during 10 days (Fig. 5C and D). These results suggest that TPCs might have an important role in heart remodeling. To further examine their role, we then chronically exposed *Tpcn1/2*$^{-/-}$ mice to isoproterenol using the same protocol. Echocardiography and ECG recordings revealed that isoproterenol modulated LVEF and FS similarly in both mouse strains, WT and *Tpcn1/2*$^{-/-}$ (Figure S6). In contrast, we observed structural changes only in WT heart but not in *Tpcn1/2*$^{-/-}$ mice. In WT mice, isoproterenol evoked a thickening of both the LV posterior wall (LVPW, Fig. 5E and F) and the interventricular septum (IVS, Fig. 5G). Determining the heart weight body weight ratio (HW/BW), isoproterenol induced heart hypertrophy of around 22 % in WT mice, which was significantly reduced in *Tpcn1/2*$^{-/-}$ mice (Fig. 5H).

3. Discussion

In this study, we demonstrate that TPCs are important for heart function, since we found that *Tpcn1/2*$^{-/-}$ mice display alterations of the LV systolic and diastolic function. At a cellular level, our data point towards a reduction in cell shortening and in the amplitude of caffeine-evoked Ca^{2+} transient in cardiomyocytes from *Tpcn1/2*$^{-/-}$ mice, associated with a dramatic reduction of the expression of important proteins involved in the SR Ca^{2+} regulation. We also found that TPCs deletion impaired adaptation to stress effort likely due to the down regulation of key metabolic regulators. Finally, in two models of cardiac hypertrophy (TAC and isoproterenol treated mice), we found a higher TPCs expression whereas their deletion (*Tpcn1/2*$^{-/-}$ mice) reduced hypertrophy induction.

Our data provide strong evidence for a role of TPCs in heart function. Indeed, *Tpcn1/2*$^{-/-}$ mice display alterations of the LV systolic function such as a reduced LVEF and reduced FS, accompanied with a LV relaxation impairment. These impairments were not due to cardiac conduction defects (evaluated by ECG). Additionally, no distinguishable major structural defects evaluated by either echocardiography, fibrosis measurement or electron microscopy were observed, thus reinforcing our hypothesis of an intrinsic cardiac function of TPCs, with no apparent effects on skeletal muscle. Moreover, we found Ca^{2+} signaling defects in isolated cardiomyocytes from *Tpcn1/2*$^{-/-}$ mice that could at least partly explain the systolic defect seen in echocardiography. Effectively, TPCs deletion led to cell shortening impairment and to a reduced amplitude of both the caffeine response and the peak post-rest, indicating a decrease in the SR Ca^{2+} content and filling capacity. Importantly, it appears that a remodeling or a change in the activity of essential proteins for the SR

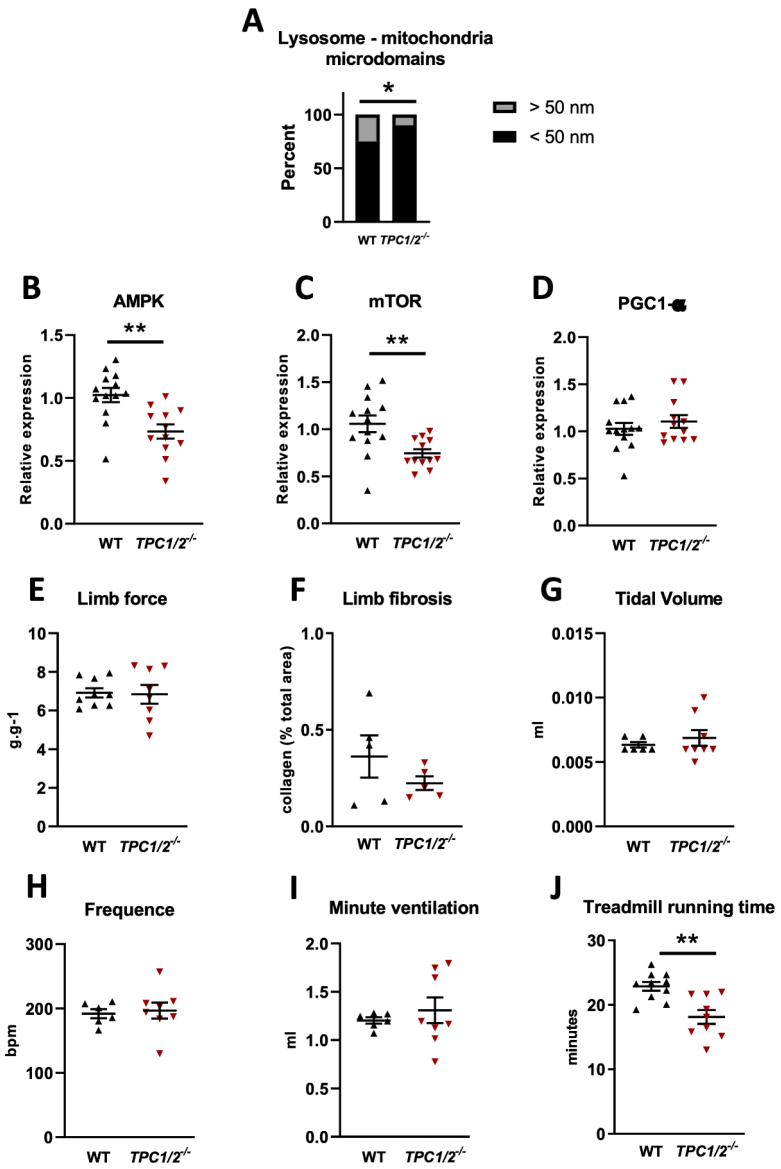

Fig. 4. ***Tpcn1/2*$^{-/-}$ mice display reduced treadmill performance, energy metabolism regulators remodeling, and no major changes in mitochondria activity. (A)** Proportion of these lysosomes forming microdomains with mitochondria (<50 nm) or not (>50 nm). Significance was assessed using a chi-square test (n = 54 lysosomes obtained from WT mice (N = 3 mice) and n = 58 lysosomes obtained from *Tpcn1/2*$^{-/-}$ mice (N = 3 mice)). **(B,C,D)** Relative expression (RT-qPCR) of AMPK, mTOR and PGC1-α in *Tpcn1/2*$^{-/-}$ mice compared with WT mice. Each dot of the graphs (B-G) represents the value (triplicate) obtained from a single mouse (N = 13 WT mice; N = 12 *Tpcn1/2*$^{-/-}$ mice). **(E)** grip strength was measured using a grip strength meter. The values were done in triplicate and normalized to mouse weight. **(F)** Dot plot showing the quantification of limb collagen staining area (% total area) revealed by Masson's trichrome staining in WT and *Tpcn1/2-/-* mice. **(G, H,I)** Dot plot showing the quantification of the plesthysmography parameters, **(G)** tidal volume, **(H)** the frequence and **(I)** the minute ventilation. **(J)** Maximum running time performed by WT and *Tpcn1/2*$^{-/-}$ mice on a treadmill. Each dot of the graph G represents a mouse and each dot value was from a single mouse run (N = 10 WT mice; N = 9 *Tpcn1/2*$^{-/-}$ mice). Values are expressed as mean ± SEM and significance: *p<0.05, **p<0.01, ***p<0.001. Significance was assessed using a t- test.

Ca^{2+} stores regulation occurred. Indeed, we observed a decrease in the expression of CSQ2 and RyR in *Tpcn1/2*$^{-/-}$ mice. Despite this RyR downregulation, functionally the Ca^{2+} transient amplitude recorded in vitro is not significantly changed in *Tpcn1/2*$^{-/-}$ cardiomyocytes. This could be partly due to the decrease of CSQ2 which led to a higher RyR activity by destabilizing this receptor, as suggested by the increase in the fractional release and the maintained occurrence of Ca^{2+} sparks and electrically evoked Ca^{2+} transients at a lower SR Ca^{2+} load (Fig. 2I). In contrast to experiments using full CSQ2-KO, that have shown huge Ca^{2+} leaks and waves [29], the *Tpcn1/2*$^{-/-}$ mice have only a modest decrease in CSQ2 which was associated with a reduced expression of RyR. This could explain why no major changes was observed in Ca^{2+} sparks and waves frequencies, monitored as an index of RyRs activity. However, since CSQ2 is the major Ca^{2+} buffer in the SR, a modest decrease in levels can directly be involved in the reduction of the total SR Ca^{2+} load mobilized by caffeine, while the free luminal Ca^{2+} would be maintained, resulting in a Ca^{2+} transient of normal amplitude [30]. Thereby and in addition with a slight increase in RyRs sensitivity, this remodeling appeared sufficient for electrical stimulation-evoked Ca^{2+} transient of amplitude comparable with those recorded in WT cardiomyocytes. From our data and from other studies, one hypothesis could explain why a decrease of the RyR and CSQ expression occurred in absence of TPCs. Indeed, our data confirmed recent high-resolution electron microscopy studies [23,31], showing that lysosomes and SR form close contacts in the nanometer range in the t-tubule domain, suggesting functional direct Ca^{2+} exchanges between these organelles, probably through the

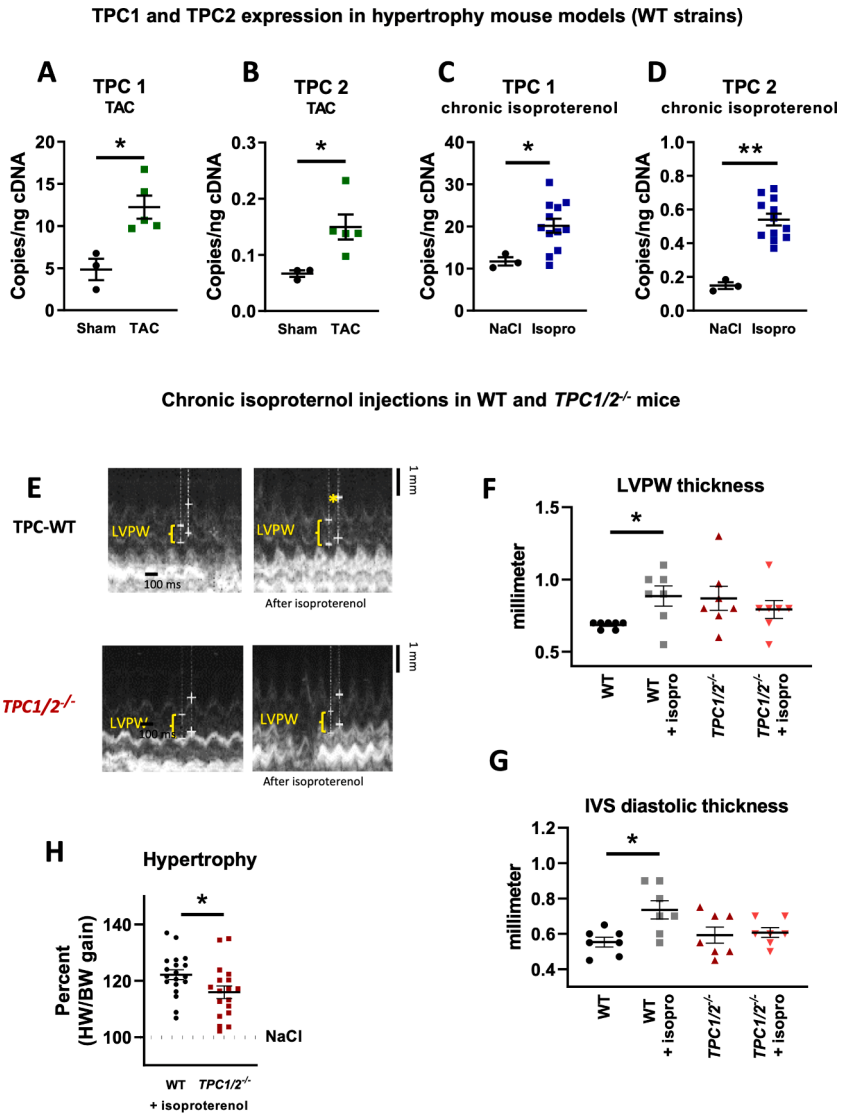

Fig. 5. TPCs are highly expressed in hypertrophic heart and their deletion reduced the heart hypertrophy induced by chronic isoproterenol injections. (A, B) Quantification by RT-qPCR of the absolute levels of *Tpcn1* and *Tpcn2* transcripts in sham mice hearts and after a TAC surgery ($N = 3$ Sham mice; $N = 5$ *TAC* mice). Each dot represents a mouse and each dot value is from triplicate. Significance was assessed using a Mann-Whitney test. **(C,D)** Quantification by RT-qPCR of the absolute levels of *Tpcn1* and *Tpcn2* transcripts in heart following chronic NaCl or isoproterenol injections of WT mice (10 days, $N = 3$ NaCl mice; $N = 12$ isoproterenol treated mice). Each dot represents a mouse and each dot value is from triplicate. Significance was assessed using a Mann-Whitney test. **(E)** Typical time motion mode echocardiography of the left ventricle from a parasternal short axis view, showing the thickness of the left ventricular posterior wall (LVPW), before and after chronic isoproterenol injections in WT and *Tpcn1/2*$^{-/-}$ mice. **(F,G)** Measure of the LVPW (yellow), interventricular septum (IVS) and the left ventricle mass, evaluated by echocardiography. Significance was assessed using a Mann-Whitney test (value was obtained in duplicate). Each dot of the graphs **(F,G)** represents a mouse ($N = 7$ WT mice; $N = 7$ WT mice + isoproterenol, $N = 7$ *Tpcn1/2*$^{-/-}$ mice, $N = 7$ *Tpcn1/2*$^{-/-}$ mice +isoproterenol). **(H)** Effect of chronic isoproterenol injections on heart hypertrophy (evaluated by the HW/BW ratio) on $N = 19$ WT and $N = 18$ *Tpcn1/2*$^{-/-}$ mice and expressed as percent of the control mice (NaCl) which represent the 100 % value. Significance was assessed using a *t*-test. Each dot of the graph represents a mouse. Significance: *$p<0.05$, **$p<0.01$, ***$p<0.001$. Significance was assessed using a *t*- test.

SERCA2 pumps and/or RyRs. Besides the ultrastructural evidence, it has also been shown that functional Ca^{2+} exchanges between the lysosomes and the SR occurs upon NAADP action [32] at microdomains formed at membrane contact sites [12]. The deletion of TPCs would have thus reduced the Ca^{2+} uptake in the SR by the SERCA2 pumps, thereby leading to a reduced expression of CSQ2 and RyRs, possibly to limit Ca^{2+} leakage from the SR. Moreover, the lower expression of NCX observed in *Tpcn1/2*$^{-/-}$ cardiomyocytes should lead to a reduced Ca^{2+} extrusion from the cytosol and might indirectly favor the SR Ca^{2+} refiling, thus compensating the reduced Ca^{2+} exchanges occurring between lysosomes and SR. All together, these results show that TPCs removal led to a new equilibrium between Ca^{2+} stores and revealed an important functional link between endolysosomal TPCs and these SR proteins. In addition, other evidences support also their role in the SR Ca^{2+} filling state. Indeed, a study showed that Ca^{2+} release from TPCs activates CaMKII to phosphorylate phospholamban upon ß-adrenergic stimulation, thereby modulating the SERCA pumps activity and thus the SR Ca^{2+} content [5]. Moreover, a recent study showed that TPCs are actually constitutively active channels [31]. Thus, TPCs could be, even in basal state condition, key actors modulating the Ca^{2+} exchanges between lysosomes and SR. Finally, we hypothesize that the relaxation impairment of heart *Tpcn1/2*$^{-/-}$ mice, seen at echocardiography, could be related to the fact that TPCs deletion led to an increase in the c-TnI expression, associated with a significant reduction of NCX.

Besides the functional link between TPCs and the SR, our electron microscopy ex-periments revealed that lysosomes are also located

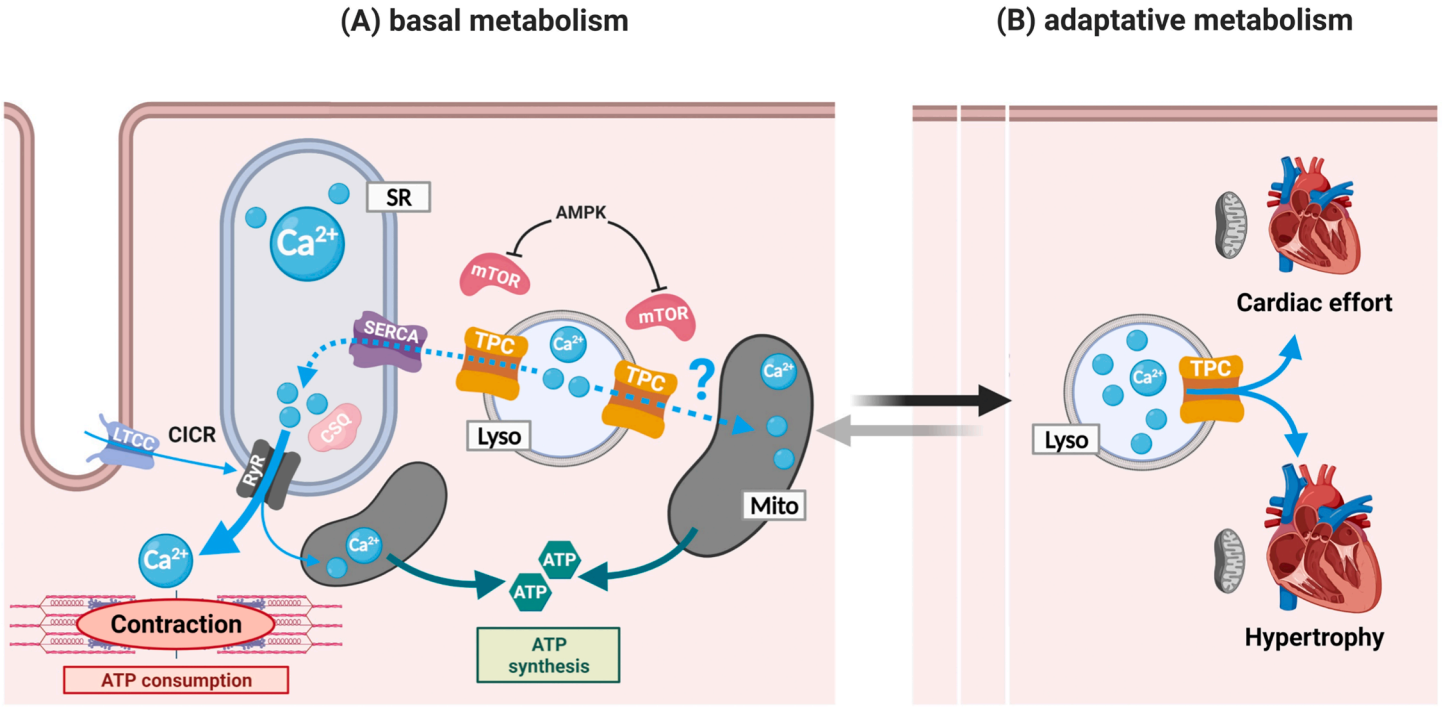

Fig. 6. Proposed scheme for actions of TPCs in cardiomyocyte. (A) TPCs release $Ca^{2+}$to participate to the shortening of the heart likely through the SR refilling requiring SERCA2 pumps activity and CSQ2, the main SR Ca^{2+} buffer as suggested by the decrease in CSQ2 expression in *Tpcn1/2*$^{-/-}$ cardiomyocytes. In this model, the Ca^{2+} released by TPCs could also be taken-up by mitochondria which produce ATP. The AMPK activation following ATP consumption leads to translocation of mTOR away from the lysosomes [41] which favors further activation of TPCs. **(B)** Scheme showing that TPCs are required for hypertrophy induction and their participation in cardiac effort likely through the Ca^{2+}-dependent modulation of the energy metabolism. CICR: Ca^{2+}-induced Ca^{2+}release; LTCC: l-type calcium channel; AMPK: AMP-activated protein kinase; SR: sarcoplasmic reticulum; Lyso: lysosome; Mito: mitochondria.

within 50 nm of mitochondria, likely forming functional nanodomains with them. Intriguingly, in cardiomyocytes from *Tpcn1/2*$^{-/-}$ mice, it appears that lysosomes are smaller and show a higher proportion in very close proximity of mitochondria, suggesting a functional link between these two organelles. Supporting this view, a recent paper has shown that lysosomal Ca2+ could be directly transferred to mitochondria [33]. Therefore, TPC-mediated lysosomal Ca2+ release could participate in the control of the energy production by mitochondria to meet the energy needs of the myocardium. It is documented that TPCs are activated and essential for autophagy under starvation and low energy status conditions. Indeed, TPCs are inhibited by mTOR translocation to the lysosomes and by high levels of ATP produced by mitochondria under the control of AMPK activity [15–17]. In contrast to a previous study which found muscle fibrosis in *TPC2*$^{-/-}$ mice due to autophagic defect [16], we observed no heart necrosis or fibrosis even with aged *Tpcn1/2*$^{-/-}$ mice (22 months old). Therefore, the basal energy status of cardiomyocytes is likely not dramatically altered when the two isoforms of TPCs are deleted However, here, we found that AMPK and mTOR expressions are reduced in *Tpcn1/2*$^{-/-}$ mice. Thus, their complex regulation and the adaptation of the energy status of the cell could be impaired in these mice, especially when the energy needs increase, which was tested by our treadmill exhaustion test which revealed that *Tpcn1/2*$^{-/-}$ mice could not perform as well as the WT mice. This last result suggests that TPCs could be important for heart adaptation to an increased workload, a process depending on both Ca^{2+} signaling and AMPK/mTOR signaling. This prompted us to see at whether TPCs are involved in two pathological models displaying adaptive heart hypertrophy. Interestingly, we found that TPC1 and TPC2 expression were increased in heart from TAC and WT mice exposed to chronic isoproterenol injections. This result, together with our chronic isoproterenol experiments in *Tpcn1/2*$^{-/-}$ mice which showed that TPCs deletion reduced the ability of isoproterenol to induce hypertrophy, suggest a selective role of TPCs in adaptive hypertrophy. Altogether, our data suggest that TPCs might be essential for heart function and metabolic adaptation to effort. We propose here a working model (Fig. 6) summarizing our findings and current knowledge where TPCs link ECC to energy metabolism.

How TPCs are recruited in cardiomyocytes remains poorly understood. Many studies have linked TPCs to the Ca^{2+} releasing messenger NAADP [34,3]. In the heart, isoproterenol has been reported to modulate Ca^{2+} transient by recruiting TPC2 in a NAADP dependent manner, likely through the activation of CD38, as a key step in ß-adrenergic receptor-mediated modulation [4–6,21]. It has been proposed that TPC2 modulate ECC, by releasing Ca^{2+} from the endo-lysosomes which then either sensitizes RyRs to facilitate CICR, or is taken up by the SERCA pumps to increase the SR Ca^{2+} load [32,5,35]. However, in our study, we found that acute ß-adrenergic modulation occurred even in absence of TPCs. Indeed, isoproterenol-induced Ca^{2+} transient and cell shortening was not altered in *Tpcn1/2*$^{-/-}$ mice suggesting that the increase of the Ca^{2+} transient and SR Ca^{2+} load known to occur upon the ß-adrenergic stimulation mostly depend on other signaling pathway such as the cAMP pathway. Nevertheless, our data on chronic isoproterenol injections clearly show that TPCs are required for the induction of hypertrophy which is a Ca^{2+} and mTOR dependent mechanisms [36]. Knowing that deletion of TPCs altered these two pathways in our study, it appears that TPCs would be key channels for long-lasting adaptive ß-adrenergic modulation rather than acute modulation of the ECC.

Overall, we have provided the first evidence that endolysosomal TPCs should now be considered as important regulators of the heart function, its adaptation and above all, that TPC1 and 2 deletion led to altered cardiac function and to important remodeling of key signaling molecules necessary for heart viability and function. Our findings may have significant clinical implications, since Ca^{2+} signaling remodeling in heart failure is highly relevant, frequent and not well understood [37]. Finally, our data highlights for the first time that TPCs inhibition could be valuable to reduce heart hypertrophy but at the expense of the resistance to fatigue. We propose therefore that we should also consider the potential benefit of stimulating TPCs therapeutically in heart disease to favor heart functioning.

4. Materials and methods

Animals: *Tpcn1/2*$^{-/-}$ mice were generated by crossing mutants homozygous for the TPC1 isoform (Tpcn1^{T159}) [38] obtained by the European Mouse Mutant Archive (EMMA) and mutants homozygous for the TPC2 isoform (Tpcn2^{YHD437})[8]. Briefly, *Tpcn1*$^{+/-}$/*Tpcn2*$^{+/-}$ mice resulting from crosses of *Tpcn1*$^{-/-}$ (TPC1 T159) with *Tpcn2*$^{-/-}$ (TPC2 YHD437) mice were further crossed for generation of WT (*Tpcn1*$^{+/+}$/*Tpcn2*$^{+/+}$) and DKO mice (*Tpcn1*$^{-/-}$/*Tpcn2*$^{-/-}$) and mice were born at the expected Mendelian proportion (8/128) and kept as separate colonies bred in our animal facility. Animal care and experimental procedures complied with the European Communities Council Directive (CEE 86/609/EEC), EU Directive 2010/63/EU, and local ethic committee (Paris Centre et Sud, N°59). Euthanasia was performed by cervical dislocation. In the case of cardiomyocyte preparations, euthanasia was achieved using anesthesia with thiopental (Dolethal®, one intraperitoneal injection at 10 μL/10 g), followed by heart removal.

Doppler – Echocardiography: Doppler echocardiography was performed in animals under isoflurane anesthesia. Anesthesia doses were kept to the lowest possible levels, usually 5 % isoflurane for induction and 1–1.5 % isoflurane during measurements. Animals were placed on a heating pad to maintain a constant body temperature (37 °C) and their rectal temperature was monitored throughout the experiment. Doppler-Echocardiography was performed using a high-resolution ultrasound system (Logiq 9, GE, France) with a 36 MHz scan head. Each animal was shaven from the left sternal border to the left axillary line with depilatory cream before the exam. Each set of measurements was obtained from the same cardiac cycle. At least three sets of measurements were obtained from three different cardiac cycles. The LV end-diastolic diameter (LVEDD), the posterior wall end diastolic thickness (PW) and the interventricular septal wall end diastolic thickness (IVS) were measured with the use of the leading-edge convention of the American Society of Echocardiography from a parasternal M mode short axis view of the LV at the papillary muscle level. Left ventricular shortening fraction and left ventricular ejection fraction (LVEF) were calculated from the M mode. Aortic velocity integral (VTI) was recorded during the procedure, from an apical view, the sample positioned in the subartic zone. Mitral inflow Doppler pattern was recorded (peak E, Peak A, deceleration time) from a 4 chambers apical view, the sample positioned at the tip of the mitral valve. The left ventricular systolic and diastolic intervals, namely the isovolumic contraction time (IVCT), the aortic ejection time (ET) and the diastolic interval of the isovolumic relaxation time (IVRT) were measured for the Tei index calculation. Measurements were made from aortic and mitral blood flows, from an apical 4 chambers modified view. The Tei index was calculated as the ratio (IVCT + IVRT)/systolic ejection time (ET). Cardiac output (CO) was defined as stroke volume x heart rate. The shortening fraction (%) was calculated by the formula: (LVEDD-LVESD)/LVEDD × 100. LV myocardial volume (LVV), LV end-diastolic (EDV) and end-systolic (ESV) volumes were calculated using a half ellipsoid model of the LV. From these volumes, LV ejection fraction (%) was calculated by the formula: (EDV-ESV)/EDV × 100.

ECG recording: The procedure was realized under isoflurane anesthesia. Anesthesia doses were kept to the lowest possible levels, usually 5 % isoflurane for induction and 1–1.5 % isoflurane during measurements. Animals were placed on a heating pad to maintain a constant body temperature (37 °C) and their rectal temperature was monitored throughout the experiment. Three-lead electrocardiography was performed (gain, 1k; A-M Systems) and band pass-filtered (100 Hz to 10 kHz). The signals were digitized with an 8-channel Powerlab data acquisition device (Acquisition rate: 100 k/s; AD Instruments) connected to a computer and analyzed using LabChart 8 Pro-software (AD Instruments). The ECG data were submitted to a 50 Hz notch filter with

an automatic setting determined by the software (ECG additional module of LabChart). Because in rodents the T wave is very close to QRS complex, the end of QRS complex of each signal was considered as T wave start.

Acute β-adrenergic stress test: After basal parameters have been recorded during hemodynamic and ECG procedures, isoproterenol (Sigma-Aldrich) was injected intraperitoneally at a single dose of 2 mg/kg. 5 min after injection, when isoproterenol effect was stabilized, hemodynamic and ECG parameters were recorded and analyzed again.

Chronic β-adrenergic stress test: Chronic β-adrenergic stimulation was sustained by subcutaneous injection of isoproterenol under light isoflurane anesthesia (5 % for 30 s). Mice were randomly assigned to receive a continuous subcutaneous infusion of isoproterenol (ISO, 10 mg/kg/day) or vehicle (0.9 % NaCl) for 10 days. At the end of the infusion period, mice were sacrificed, body and heart were weighted.

Cardiomyocytes preparation and Ca^{2+} imaging: Cardiomyocyte preparations were obtained by enzymatic dissociation according to the method of Langendorff, as previously described [39]. Cardiomyocytes functioning was evaluated by using a classic protocol of cell electrical stimulation at 2 Hz. Each electrical stimulation gives rise to a cytosolic Ca^{2+} elevation called Ca^{2+} transient which is visualized by confocal microscopy (Leica SP5) in "line-scanning mode" in cardiomyocytes loaded with the calcium sensitive dye Fluo-3-AM as previously described (Zelicourt, 2022). The cytosolic Ca^{2+} variation was normalized by dividing the peak fluorescence intensity (F) by the average resting fluorescence intensity (F_0) after background subtraction. For SR Ca^{2+} load estimation, cardiomyocytes were rapidly perfused with 10 mM caffeine immediately after field stimulation. The amplitude of the caffeine-evoked $[Ca^{2+}]$i transients was used to assess the SR Ca^{2+} load. Fractional SR release was measured by normalizing the steady state of $[Ca^{2+}]$i transients (peak F/F_0) to that of caffeine-evoked $[Ca^{2+}]$i transients. Post-rest potentiation was calculated by normalizing the first $[Ca^{2+}]$i transients (peak F/F_0) after a period of rest to reach the steady-state $[Ca^{2+}]$i transients. $[Ca^{2+}]$i transient properties and the amplitude (maximum F/F_0) were calculated by using the IDL software with a homemade program.

Ca^{2+} spark and wave recordings: To record spontaneous Ca^{2+} sparks and Ca^{2+} waves in intact quiescent cells, each myocyte was scanned at 1.5 ms per line. Ca^{2+} sparks were detected as localized, rapid, and brief elevations in Ca^{2+} fluorescence. Ca^{2+} sparks were detected using an automated detection system (homemade in IDL; Exelis Visual Information Solutions) and a criterion that limited the detection of false events while detecting most Ca^{2+} sparks [40]. Spontaneous Ca^{2+} release manifested as Ca^{2+} waves were quantified by the percentage of occurrence. Ca^{2+} wave was identified as an increase in the Ca^{2+} fluorescence starting locally and propagated to one or both sides of the cell.

Western blot: Total heart homogenate and total mitochondrial proteins were resolved on 4–15 % Tris-glycine SDS-PAGE gels and electroblotted onto polyvinylidene fluoride (PVDF) membranes (Bio-Rad, Marnes La Coquette, France). Following electrotransfer, membranes were blocked for 1 h at room temperature in 5 % BSA-PBST (10 mM Tris–HCl, pH 8.0/ 150 mM NaCl/0.1 % Tween 20). Next, membranes were incubated overnight at 4 °C with primary antibody. Then, the membranes were washed six times with PBST and incubated with peroxidase-conjugated secondary antibody at room temperature for 1 h. Peroxidase activity was detected with enhanced chemiluminescence (ECL Advance Western blotting detection kit; Thermo Scientific, Villebon sur Yvette, France). For protein detection, the following antibodies were used: anti-CaV 1.2 (Millipore, AB5156), anti-RyR2 Total (Thermo Fisher Scientific, MA3–916), anti-phosphoRyR2 Ser2808 (Badrilla, A010–30AP), anti-NCX (Swant, R3F1) anti-calsequestrin (Thermo Fisher Scientific, PA1–913), anti-SERCA2 total (Santa Cruz, sc-515,162), anti-troponin-I (Cell Signaling, 4002), anti-PLB total (Thermo Fisher Scientific, MA3–922), anti-phosphoPLB-Thr17 (Badrilla, A010–13), anti-phosphoPLB-Ser16 (Badrilla, A Q10–12), anti-troponin-C (Invitrogen, PA5 76,641), anti-vinculin (Sigma, V9131), anti-actin (Sigma, A2066), anti-GAPDH (Cell Signaling, 2118).

Combined forelimb and hindlimb grip strength measurement: Grip strength was measured using a grip strength meter (Bioseb, Vitrolles, France). The apparatus consisted of a grid connected to a digital dynamometer. The animals were gently lowered over the top of the grid so that both sets of front paws and hind paws could grip the grid. While the torso of the animal was kept parallel to the grid, the mouse was gently pulled back by the tail until it released its grip. This procedure was repeated 3 times, the maximum and the mean values have been normalized to mouse body weight.

Barometric plethysmography: The respiratory function of mice was evaluated by whole-body plethysmography using an EMKA technologies plethysmograph, essentially as described by TREAT-NMD. Briefly, unrestrained conscious mice were placed in calibrated animal chambers and the pressure difference between the reference and animal chambers was measured using a pressure transducer. Mice were allowed to acclimate in the chambers for 45 min at stable temperature and humidity. Data were then collected every 5 s using the iox2 software (version 2.8.0.19; EMKA technologies). The inspiration time (TI) was defined as the time from the start of inspiration to the end of inspiration and the expiration time (TE) was defined as the time from the start of expiration to the end of expiration. The relaxation time (RT) was defined as the time from the start of expiration to the time when 65 % of the total expiratory pressure occurred. Pause and enhanced pause (penh) were defined and calculated by the following formulas: $\text{Pause} = (\text{TE} - \text{RT})/\text{RT}$ and $\text{penh} = (\text{PEP}/\text{PIP}) \times \text{Pause}$, where PEP is peak expiratory pressure and PIP is peak inspiratory pressure. The value of each parameter was calculated from an average of 60 recordings of 5 s representing a total of 5 min. Inclusion criteria for each recording were >8 respiration events by 5 s and >80 % of success rate as measured.

Treadmill exercise: Endurance was characterized by measuring running time, distance and maximal running speed, using a motorized treadmill (Columbus Instruments). The mice were acclimated to the treadmill for 2 consecutive days, 15 min per day, 5 min at rest and 10 min at a speed of 10 cm/*sec* and a grade of 0 %. The following day, animals ran on the treadmill at an initial speed of 10 cm/*sec* (0 % grade) for 5 min, after which the speed was increased by 1 cm/*sec* every subsequent 30 s, until the mice were exhausted. Exhaustion was defined as the inability of the mouse to remain on the treadmill despite a mechanical prodding.

RNA isolation and RT-qPCR: RNA isolation: total RNAs from frozen hearts were isolated using Trizol (Invitrogen) extraction according to the manufacturer instructions. For each sample, total isolated RNA was quantified using the Implen NanoPhotometer® N120. Reverse transcription (cDNA synthesis) was performed using the SuperScript III Reverse Transcriptase (Invitrogen). The samples were prepared as follows: 10 μL RTMix (2x) + 2 μL RT Enzyme + 1,5 μg d'ARN, H_2O QSP 20uL. The samples were placed in the Biorad T100 Thermal Cycler for 10 min at 25 °C, then 30 min at 50 °C, and 5 min at 85 °C. RTqPCR was performed according to the SYBR Green protocol (BioRad), in triplicate on the CFX384 Touch Real-Time detection system (BioRad) using iTaq Universal SYBR Green Supermix (BioRad). The following cycling parameters were used: 50 C (2 min), 95 C (10 min), 40 cycles of 95 C (15 s) and 60 C (1 min), followed by cooling at 40 C (30 s). The following primers were used: Tpcn1 (F: CTGTCCTCTGGATGGAACCT; R: TCCATGTTGAGCGT CAGTG), Tpcn2 (F: CCCTGGCTGTATACCGATTG; R: GTCCCA GAGCGACAGTGG), mTOR (F: AGAAGGGTCTCCAAGGACGACT ; R : GCAGGACACAAAGGCAGCATTG), AMPK (F : CGCCTCTAGTCCTCCATCAG ; R : ATGTCACACGCTTTGCTCTG), PGC-1alpha (F : AAGTGTGGAACTCTCTGGAACTG ; R : GGGTTATCTTGGTTGGCTTTATG), GAPDH (F : TGACGTGCCGCCTGGAGAAA ; R : AGTGTAGCCCAAGATGCCCTTCAG). For *Tpcn1/2* cDNA copy numbers were determined against a standard curve using a custom-made double-stranded DNA fragment containing the amplicon sequences for Tpcn1 and Tpcn2 as described in [11] . Expression of mRNA was normalized to GAPDH mRNA expression. Differences in gene

expression were determined using the $2^{-\Delta\Delta C}{}_{T}$ method, and reported as fold change (relative to WT).

Masson's trichrome staining: Cryostat muscle sections (10 μm) were stained with Masson's trichrome to visualize connective tissue and muscle fibers in pink and collagen in blue (Sigma kit HT15; Sigma-Aldrich) and then observed using a scanner Leica Aperio® AT2 (Leica Microsystems). Fibrotic tissue invaded by collagen (stained in blue) was quantified using the Aperio Image Analysis IHC Leica.

Electron microscopy: Left ventricular papillary muscles were isolated from three control and three KO mouse hearts, fixated with 2 % glutaraldehyde in cacodylate buffer (in mM: 150 Na-Cacodylate, 2 CaCl2, pH 7.3) for 1 h, post-fixated by 1 % osmium tetroxide in cacodylate buffer for 30 min and stained with 1 % aqueous solution of uranyl acetate. After dehydration in graded ethanol series and acetone, the tissue was embedded in Durcupan (ACM Fluka). Sections (70 nm) were cut using a diamond knike (Diatome) on a Leica UC6 ultramicrotome. The sections were collected on formvar-carbon coated copper grids before to be contrasted with 2 % uranyl acetate (10 min) and Reynold's lead citrate (2 min). Sections were observed with a TEM JEOL1400 electron microscope operating at 80 kV or 120 kV. Raw images were analyzed with ImageJ software.

Statistics: For each quantitative data set, an outlier research has been performed using the ROUT method ($Q = 1$ %). Identified outliers were removed from the analysis. Quantitative data were firstly tested for normality by D'agostino-Pearson, Shapiro-Wilk and Kolmogorov-Smirnov tests. When the distribution was normal with sample size sufficient, a student *t*-test was used otherwise the non-parametric Mann-Whitney test (two-tailed). To compare two contingencies (distributions), a chi-square test was performed (Fig 3D; S4A). Values are expressed as mean ± SEM and significance: $*p<0.05$, $**p<0.01$, $***p<0.001$.

CRediT authorship contribution statement

Antoine de Zélicourt: Conceptualization, Formal analysis, Investigation, Writing – review & editing, Writing – original draft. **Abdallah Fayssoil:** Formal analysis, Investigation, Validation, Writing – review & editing. **Arnaud Mansart:** Formal analysis, Investigation, Writing – review & editing. **Faouzi Zarrouki:** Formal analysis, Investigation, Writing – review & editing. **Ahmed Karoui:** Formal analysis, Investigation, Writing – review & editing. **Jérome Piquereau:** Formal analysis, Investigation, Validation, Writing – review & editing. **Florence Lefebvre:** Investigation, Writing – review & editing. **Pascale Gerbaud:** Formal analysis, Investigation, Writing – review & editing. **Delphine Mika:** Formal analysis, Investigation, Writing – review & editing. **Mbarka Dakouane-Giudicelli:** Formal analysis, Investigation, Writing – review & editing. **Erwan Lanchec:** Conceptualization, Investigation, Writing – review & editing. **Miao Feng:** Investigation, Writing – review & editing. **Véronique Leblais:** Funding acquisition, Writing – review & editing. **Régis Bobe:** Formal analysis, Funding acquisition, Investigation, Writing – review & editing. **Jean-Marie Launay:** Formal analysis, Investigation, Writing – review & editing. **Antony Galione:** Resources, Writing – review & editing. **Ana Maria Gomez:** Conceptualization, Formal analysis, Funding acquisition, Supervision, Writing – original draft, Writing – review & editing. **Sabine de la Porte:** Conceptualization, Formal analysis, Funding acquisition, Investigation, Project administration, Supervision, Validation, Writing – original draft, Writing – review & editing. **José-Manuel Cancela:** Conceptualization, Funding acquisition, Project administration, Supervision, Validation, Writing – original draft, Writing – review & editing.

Declaration of Competing Interest

None.

Data availability

Data will be made available on request.

Acknowledgments

This research has been supported by grants from CNRS, INSERM, and Paris-Saclay University. Funding for this work was provided by AFM-telethon grants (JMC, SDP, AZ). AZ is a recipient of a PhD fellowship from Paris-Sud University. This work was also partly funded by the Fondation de France (JMC, RB), AFM (JMC, SDP). INSERM U1180 is a member of the Laboratory of Excellence LERMIT supported by a grant from ANR (ANR-10-LABX-33) under the program 'Investissements d'Avenir' ANR-11-IDEX-0003–01. The authors thank the radiology department of Raymond Poincaré hospital, the electronic microscopy facility of Imagerie-Gif, supported by "France-BioImaging" (ANR-10-INBS-04–01), and the Labex "Saclay Plant Science" (ANR-11-IDEX-0003–02).

Supplementary materials

Supplementary material associated with this article can be found, in the online version, at doi:10.1016/j.ceca.2023.102839.

References

[1] D.A. Eisner, J.L. Caldwell, K. Kistamás, A.W. Trafford, Calcium and excitation-contraction coupling in the heart, Circ. Res. 121 (2017) 181–195, https://doi.org/10.1161/CIRCRESAHA.117.310230.

[2] J.M. Cancela, G. Charpentier, O.H. Petersen, Co-ordination of Ca(2+) signalling in mammalian cells by the new Ca(2+)-releasing messenger NAADP, Pflugers Arch. 446 (2003) 322–327, https://doi.org/10.1007/s00424-003-1035-x.

[3] A. Galione, NAADP receptors, Cold Spring Harb. Perspect. Biol. (2019), https://doi.org/10.1101/cshperspect.a035071.

[4] A.M. Lewis, P.K. Aley, A. Roomi, J.M. Thomas, R. Masgrau, C. Garnham, K. Shipman, C. Paramore, D. Bloor-Young, L.E.L. Sanders, D.A. Terrar, A. Galione, G.C. Churchill, β-Adrenergic receptor signaling increases NAADP and cADPR levels in the heart, Biochem. Biophys. Res. Commun. 427 (2012) 326–329, https://doi.org/10.1016/j.bbrc.2012.09.054.

[5] R.A. Capel, E.L. Bolton, W.K. Lin, D. Aston, Y. Wang, W. Liu, X. Wang, R.-A. B. Burton, D. Bloor-Young, K.T. Shade, M. Ruas, J. Parrington, G.C. Churchill, M. Lei, A. Galione, D.A. Terrar, Two-pore channels (TPC2s) and nicotinic acid adenine dinucleotide phosphate (NAADP) at lysosomal-sarcoplasmic reticular junctions contribute to acute and chronic β-adrenoceptor signaling in the heart, J. Biol. Chem. 290 (2015) 30087–30098, https://doi.org/10.1074/jbc.M115.684076.

[6] R. Gul, D.R. Park, A.I. Shawl, S.Y. Im, T.S. Nam, S.H. Lee, J.K. Ko, K.Y. Jang, D. Kim, U.H. Kim, Nicotinic Acid Adenine Dinucleotide Phosphate (NAADP) and cyclic ADP-ribose (cADPR) mediate Ca2+ signaling in cardiac hypertrophy induced by β-adrenergic Stimulation, PLoS One 11 (2016), e0149125, https://doi.org/10.1371/journal.pone.0149125.

[7] W.K. Lin, E.L. Bolton, W.A. Cortopassi, Y. Wang, F. O'Brien, M. Maciejewska, M. P. Jacobson, C. Garnham, M. Ruas, J. Parrington, M. Lei, R. Sitsapesan, A. Galione, D.A. Terrar, Synthesis of the Ca2+-mobilizing messengers NAADP and cADPR by intracellular CD38 enzyme in the mouse heart: role in β-adrenoceptor signaling, J. Biol. Chem. 292 (2017) 13243–13257, https://doi.org/10.1074/jbc.M117.789347.

[8] P.J. Calcraft, M. Ruas, Z. Pan, X. Cheng, A. Arredouani, X. Hao, J. Tang, K. Rietdorf, L. Teboul, K.T. Chuang, P. Lin, R. Xiao, C. Wang, Y. Zhu, Y. Lin, C.N. Wyatt, J. Parrington, J. Ma, A.M. Evans, A. Galione, M.X. Zhu, NAADP mobilizes calcium from acidic organelles through two-pore channels, Nature 459 (2009) 596–600, https://doi.org/10.1038/nature08030.

[9] E. Brailoiu, D. Churamani, X. Cai, M.G. Schrlau, G.C. Brailoiu, X. Gao, R. Hooper, M.J. Boulware, N.J. Dun, J.S. Marchant, S. Patel, Essential requirement for two-pore channel 1 in NAADP-mediated calcium signaling, J. Cell Biol. 186 (2009) 201–209, https://doi.org/10.1083/jcb.200904073.

[10] X. Zong, M. Schieder, H. Cuny, S. Fenske, C. Gruner, K. Rötzer, O. Griesbeck, H. Harz, M. Biel, C. Wahl-Schott, The two-pore channel TPCN2 mediates NAADP-dependent Ca(2+)-release from lysosomal stores, Pflugers Arch. 458 (2009) 891–899, https://doi.org/10.1007/s00424-009-0690-y.

[11] M. Ruas, L.C. Davis, C.C. Chen, A.J. Morgan, K.T. Chuang, T.F. Walseth, C. Grimm, C. Garnham, T. Powell, N. Platt, F.M. Platt, M. Biel, C. Wahl-Schott, J. Parrington, A. Galione, Expression of Ca^{2+}-permeable two-pore channels rescues NAADP signalling in TPC-deficient cells, EMBO J. 34 (2015) 1743–1758, https://doi.org/10.15252/embj.201490009.

[12] C.J. Penny, B.S. Kilpatrick, E.R. Eden, S. Patel, Coupling acidic organelles with the ER through Ca^{2+} microdomains at membrane contact sites, Cell Calcium 58 (2015) 387–396, https://doi.org/10.1016/j.ceca.2015.03.006.
[13] K. Ishibashi, M. Suzuki, M. Imai, Molecular cloning of a novel form (two-repeat) protein related to voltage-gated sodium and calcium channels, Biochem. Biophys. Res. Commun. 270 (2000) 370–376, https://doi.org/10.1006/bbrc.2000.2435.
[14] X. Wang, X. Zhang, X.P. Dong, M. Samie, X. Li, X. Cheng, A. Goschka, D. Shen, Y. Zhou, J. Harlow, M.X. Zhu, D.E. Clapham, D. Ren, H. Xu, TPC proteins are phosphoinositide- activated sodium-selective ion channels in endosomes and lysosomes, Cell 151 (2012) 372–383, https://doi.org/10.1016/j.cell.2012.08.036.
[15] C. Cang, Y. Zhou, B. Navarro, Y.J. Seo, K. Aranda, L. Shi, S. Battaglia-Hsu, I. Nissim, D.E. Clapham, D. Ren, mTOR regulates lysosomal ATP-sensitive two-pore Na(+) channels to adapt to metabolic state, Cell 152 (2013) 778–790, https://doi.org/10.1016/j.cell.2013.01.023.
[16] P.H. Lin, P. Duann, S. Komazaki, K.H. Park, H. Li, M. Sun, M. Sermersheim, K. Gumpper, J. Parrington, A. Galione, A.M. Evans, M.X. Zhu, J. Ma, Lysosomal two-pore channel subtype 2 (TPC2) regulates skeletal muscle autophagic signaling, J. Biol. Chem. 290 (2015) 3377–3389, https://doi.org/10.1074/jbc.M114.608471.
[17] V. García-Rúa, S. Feijóo-Bandín, D. Rodríguez-Penas, A. Mosquera-Leal, E. Abu-Assi, A. Beiras, L. María Seoane, P. Lear, J. Parrington, M. Portolés, E. Roselló-Lletí, M. Rivera, O. Gualillo, V. Parra, J.A. Hill, B. Rothermel, J.R. González-Juanatey, F. Lago, Endolysosomal two-pore channels regulate autophagy in cardiomyocytes, J. Physiol. (Lond.). 594 (2016) 3061–3077, https://doi.org/10.1113/JP271332.
[18] M. Schieder, K. Rötzer, A. Brüggemann, M. Biel, C.A. Wahl-Schott, Characterization of two-pore channel 2 (TPCN2)-mediated Ca2+ currents in isolated lysosomes, J. Biol. Chem. 285 (2010) 21219–21222, https://doi.org/10.1074/jbc.C110.143123.
[19] S.J. Pitt, A.K.M. Lam, K. Rietdorf, A. Galione, R. Sitsapesan, Reconstituted human TPC1 is a proton-permeable ion channel and is activated by NAADP or Ca2+, Sci. Signal 7 (2014) ra46, https://doi.org/10.1126/scisignal.2004854.
[20] L. Lagostena, M. Festa, M. Pusch, A. Carpaneto, The human two-pore channel 1 is modulated by cytosolic and luminal calcium, Sci. Rep. 7 (2017) 43900, https://doi.org/10.1038/srep43900.
[21] M. Nebel, A.P. Schwoerer, D. Warszta, C.C. Siebrands, A.C. Limbrock, J. M. Swarbrick, R. Fliegert, K. Weber, S. Bruhn, M. Hohenegger, A. Geisler, L. Herich, S. Schlegel, L. Carrier, T. Eschenhagen, B.V.L. Potter, H. Ehmke, A. H. Guse, Nicotinic acid adenine dinucleotide phosphate (NAADP)-mediated calcium signaling and arrhythmias in the heart evoked by β-adrenergic stimulation, J. Biol. Chem. 288 (2013) 16017–16030, https://doi.org/10.1074/jbc.M112.441246.
[22] S.M. Davidson, K. Foote, S. Kunuthur, R. Gosain, N. Tan, R. Tyser, Y.J. Zhao, R. Graeff, A. Ganesan, M.R. Duchen, S. Patel, D.M. Yellon, Inhibition of NAADP signalling on reperfusion protects the heart by preventing lethal calcium oscillations via two-pore channel 1 and opening of the mitochondrial permeability transition pore, Cardiovasc. Res. 108 (2015) 357–366, https://doi.org/10.1093/cvr/cvv226.
[23] D. Aston, R.A. Capel, K.L. Ford, H.C. Christian, G.R. Mirams, E.A. Rog-Zielinska, P. Kohl, A. Galione, R.A.B. Burton, D.A. Terrar, High resolution structural evidence suggests the Sarcoplasmic Reticulum forms microdomains with Acidic Stores (lysosomes) in the heart, Sci. Rep. 7 (2017) 40620, https://doi.org/10.1038/srep40620.
[24] P.R. Territo, S.A. French, M.C. Dunleavy, F.J. Evans, R.S. Balaban, Calcium activation of heart mitochondrial oxidative phosphorylation: rapid kinetics of mVO2, NADH, AND light scattering, J. Biol. Chem. 276 (2001) 2586–2599, https://doi.org/10.1074/jbc.M002923200.
[25] L. Galluzzi, E.H. Baehrecke, A. Ballabio, P. Boya, J.M. Bravo-San Pedro, F. Cecconi, A.M. Choi, C.T. Chu, P. Codogno, M.I. Colombo, A.M. Cuervo, J. Debnath, V. Deretic, I. Dikic, E.L. Eskelinen, G.M. Fimia, S. Fulda, D.A. Gewirtz, D.R. Green, M. Hansen, J.W. Harper, M. Jäättelä, T. Johansen, G. Juhasz, A.C. Kimmelman, C. Kraft, N.T. Ktistakis, S. Kumar, B. Levine, C. Lopez-Otin, F. Madeo, S. Martens, J. Martinez, A. Melendez, N. Mizushima, C. Münz, L.O. Murphy, J.M. Penninger, M. Piacentini, F. Reggiori, D.C. Rubinsztein, K.M. Ryan, L. Santambrogio, L. Scorrano, A.K. Simon, H.U. Simon, A. Simonsen, N. Tavernarakis, S.A. Tooze, T. Yoshimori, J. Yuan, Z. Yue, Q. Zhong, G. Kroemer, Molecular definitions of autophagy and related processes, EMBO J. 36 (2017) 1811–1836, https://doi.org/10.15252/embj.201796697.
[26] R. Ventura-Clapier, A. Garnier, V. Veksler, Transcriptional control of mitochondrial biogenesis: the central role of PGC-1alpha, Cardiovasc. Res. 79 (2008) 208–217, https://doi.org/10.1093/cvr/cvn098.
[27] V.G. Zaha, L.H. Young, AMP-activated protein kinase regulation and biological actions in the heart, Circ. Res. 111 (2012) 800–814, https://doi.org/10.1161/CIRCRESAHA.111.255505.
[28] J.B. Xue, A. Val-Blasco, M. Davoodi, S. Gómez, Y. Yaniv, J.P. Benitah, A.M. Gómez, Heart failure in mice induces a dysfunction of the sinus node associated with reduced CaMKII signaling, J. Gen. Physiol. 154 (2022), e202112895, https://doi.org/10.1085/jgp.202112895.
[29] R.M. Murphy, J.P. Mollica, N.A. Beard, B.C. Knollmann, G.D. Lamb, Quantification of calsequestrin 2 (CSQ2) in sheep cardiac muscle and Ca2+-binding protein changes in CSQ2 knockout mice, Am. J. Physiol. Heart Circ. Physiol. 300 (2011) H595–H604, https://doi.org/10.1152/ajpheart.00902.2010.
[30] M. Denegri, J.E. Avelino-Cruz, S. Boncompagni, S.A. De Simone, A. Auricchio, L. Villani, P. Volpe, F. Protasi, C. Napolitano, S.G. Priori, Viral gene transfer rescues arrhythmogenic phenotype and ultrastructural abnormalities in adult calsequestrin-null mice with inherited arrhythmias, Circ. Res. 110 (2012) 663–668, https://doi.org/10.1161/CIRCRESAHA.111.263939.
[31] B.S. Kilpatrick, E.R. Eden, L.N. Hockey, E. Yates, C.E. Futter, S. Patel, An endosomal NAADP-sensitive two-pore Ca2+ channel regulates er-endosome membrane contact sites to control growth factor signaling, Cell Rep. 18 (2017) 1636–1645, https://doi.org/10.1016/j.celrep.2017.01.052.
[32] A. Macgregor, M. Yamasaki, S. Rakovic, L. Sanders, R. Parkesh, G.C. Churchill, A. Galione, D.A. Terrar, NAADP controls cross-talk between distinct Ca2+ stores in the heart, J. Biol. Chem. 282 (2007) 15302–15311, https://doi.org/10.1074/jbc.M611167200.
[33] W. Peng, Y.C. Wong, D. Krainc, Mitochondria-lysosome contacts regulate mitochondrial Ca2+ dynamics via lysosomal TRPML1, PNAS 117 (2020) 19266–19275, https://doi.org/10.1073/pnas.2003236117.
[34] S. Patel, Function and dysfunction of two-pore channels, Sci. Signal 8 (2015) re7, https://doi.org/10.1126/scisignal.aab3314.
[35] Z. Meng, R.A. Capel, S.J. Bose, E. Bosch, S. de Jong, R. Planque, A. Galione, R.A. B. Burton, A. Bueno-Orovio, Lysosomal calcium loading promotes spontaneous calcium release by potentiating ryanodine receptors, Biophys. J. 122 (2023) 3044–3059, https://doi.org/10.1016/j.bpj.2023.06.007.
[36] S.C. Bairwa, N. Parajuli, J.R.B. Dyck, The role of AMPK in cardiomyocyte health and survival, Biochim. Biophys. Acta 1862 (2016) 2199–2210, https://doi.org/10.1016/j.bbadis.2016.07.001.
[37] G.L. Smith, D.A. Eisner, Calcium buffering in the heart in health and disease, Circulation 139 (2019) 2358–2371, https://doi.org/10.1161/CIRCULATIONAHA.118.039329.
[38] M. Ruas, K.T. Chuang, L.C. Davis, A. Al-Douri, P.W. Tynan, R. Tunn, L. Teboul, A. Galione, J. Parrington, TPC1 has two variant isoforms, and their removal has different effects on endo-lysosomal functions compared to loss of TPC2, Mol. Cell. Biol. 34 (2014) 3981–3992, https://doi.org/10.1128/MCB.00113-14.
[39] J.P. Bénitah, E. Perrier, A.M. Gómez, G. Vassort, Effects of aldosterone on transient outward K+ current density in rat ventricular myocytes, J. Physiol. (Lond.). 537 (2001) 151–160, https://doi.org/10.1111/j.1469-7793.2001.0151k.x.
[40] M. Fernández-Velasco, A. Rueda, N. Rizzi, J.P. Benitah, B. Colombi, C. Napolitano, S.G. Priori, S. Richard, A.M. Gómez, Increased Ca2+ sensitivity of the ryanodine receptor mutant RyR2R4496C underlies catecholaminergic polymorphic ventricular tachycardia, Circ. Res. 104 (2009) 201–209, https://doi.org/10.1161/CIRCRESAHA.108.177493, 12p following 209.
[41] D.M. Sabatini, Twenty-five years of mTOR: uncovering the link from nutrients to growth, Proc. Natl. Acad. Sci. U.S.A. 114 (2017) 11818–11825, https://doi.org/10.1073/pnas.1716173114.